Available online at www.sciencedirect.com

jmr&t Journal of Materials Research and Technology

www.jmrt.com.br

Original Article

Bubble behavior in the slab continuous casting mold: Physical and mathematical model

Paulo Luiz Santos Jr. (Dr.)[a,c,*], *Johne Jesus Mol Peixoto (Dr.)*[b], *Carlos Antônio da Silva (PhD.)*[b], *Itavahn Alves da Silva (Dr.)*[b], *Clenice Moreira Galinari (Dr.)*[c]

[a] *RHI Magnesita/Department of Metallurgical Engineering — Pontifical Catholic University of Minas Gerais, Av. D. José Gaspar, 500, Belo Horizonte, MG, 30535-901, Brazil*

[b] *Department of Metallurgical Engineering and Materials, Federal University of Ouro Preto, Morro do Cruzeiro, Ouro Preto, MG 35400-000, Brazil*

[c] *RHI Magnesita, Praça Louis Ensch, 240, Contagem, MG 32210-902, Brazil*

ARTICLE INFO

Article history:
Received 31 October 2019
Accepted 28 February 2020
Available online 20 March 2020

Keywords:
Mathematical modeling
CFD
Continuous casting
Upper nozzle refractory
Drag and non-drag forces
Physical modeling

ABSTRACT

A two phase population balance is used to predict the polydispersed bubble flow and size distribution in a slab continuous casting mold and Submerged Entry Nozzle (SEN) system. Multiple Size Group (MUSIG) with a suitable breakage and coalescence model (Ansys CFX) was adopted to account for the polydispersed gas flow. Initial bubble size distribution as determined for two industrial refractories have been taken in consideration. A two way coupling model including the effect of the drag force and non-drag forces such as virtual mass force and turbulent dispersion force was considered. The results are compared with gas distribution in a 1:1 scale water — air mold model running under conditions of fluidynamic similarity to validate the model. The simulations have then been extended to describe the actual steel — argon flow, considering a thermal expansion factor for argon bubbles. The effect of gas distribution on the flow field of liquid inside the mold and other metallurgical aspects are discussed.

1. Introduction

Nowadays many steel grades are required to be almost defect free having a high degree of cleanliness. This aspect of stringent quality led to considerable efforts in quality control and innovations in continuous casting, and subsequent development of new products and refractory designs to support these demands. The injection of argon through the refractories, mainly through the upper nozzle, plays a fundamental role in controlling the obstruction and improving the surface temperature of the steel in the mold as well as promoting separation of non-metallic inclusions, according to Suzuki et al. [1] and Yuan et al. [2]. Many researchers have observed bubble behavior in physical models of continuous casting. Thomas et al. [3] as an example observed that gas injected from a single pore

* *Corresponding author.*
E-mails: paulo.junior@rhimagnesita.com, pauloluiz@pucminas.br (P.L. Santos Jr.), johnepeix@yahoo.com.br (J.J. Peixoto), casilva@ufop.edu.br (C.A. Silva), itavahnufop@yahoo.com.br (I.A. Silva), clenice.galinari@rhimagnesita.com (C.M. Galinari).
https://doi.org/10.1016/j.jmrt.2020.02.099

presented different bubble shapes and behaviors depending on flow rate of water and gas injection rate. Lee et al. [4] investigated the initial behavior of bubbles in a water model through filming the upper nozzle region with high-speed camera 4000 frames per second. The size of the bubble is reduced with increasing liquid velocity and becomes larger with increasing gas injection rate as it was also confirmed by Santos et al. [5] in an 1:1 scale physical model. Liu and Thomas [6] pointed out that for dynamic systems the fluid flow has a decisive effect on the size of the bubble, i.e., for higher flow rates the bubble is released from the surface of the refractory in advance with a smaller bubble diameter than in the case of reduced flow rates or in a static condition. Santos et al. [7] carried out a study to investigate the formation, behavior and to assess the dimensions of the gas bubbles inside a liquid flow system, simulating the refractory system. Refractory plates, with different characteristics, produced from industrial recipes have been used and the effect of the refractory and the gas and liquid flow rates were discussed.

Santos et al. [8] implemented a mathematical model where the effect of gas and liquid flow rate as well as non-drag forces such as wall lubrication force (WLF), turbulent dispersion force (TDF) and virtual mass force (VMF) on gas distribution were evaluated and the best setup was reached comparing the results to the physical model built for this purpose. These non-drag forces are important in order to better adjust the numerical model; this aspect has been discussed by Peixoto et al. [9] [15], Chen et al. [10] and Díaz et al. [11], Cho and Thomas [12] and Liu et al. [13] performed physical and mathematical simulations using a 1/3th scale water model in order to investigate argon bubble behavior and size distribution.

This contribution builds on previous works related to the behavior of the water — air system in a 1:1 scale mold physical model [5], to the influence of the permeability of refractory and fluids flow rates on the bubble size distribution [7] and also to physical and mathematical simulations performed to evaluate the effects of drag and non-drag forces [8] on two phase flow. A mathematical model of the SEN — mold system, using a previously determined bubble size distribution [7], with MUSIG (Multiple Size Group function — Ansys [14]), and also taking in account drag and non-drag forces [8], was developed and adjusted by comparison with results from a 1:1 scale water-air model of a SEN-Mold system. Then the simulations are expanded to include molten steel — argon system by having gas thermal expansion in account. The effect of gas distribution on the flow field of liquid inside the mold and other metallurgical aspects are discussed.

2. Methods and materials

A 1:1 scale mold physical model with 1260 mm width and 200 mm thickness is used for flow validation. Commercial upper refractory nozzle and a 1:1 scale SEN model made of acrylic are used (Fig. 1), more details are given in reference [5]. The upper nozzle and the SEN were assembled following a configuration similar to an actual slab continuous casting machine. However, some adjustments were done, such as: the SEN has two parts, one representing the SEN and other the Monoblock, the flow control is performed by a valve below the reservoir and not by a slide gate system.

The water flow rate was controlled using a paddlewheel magnetic flowmeter and a frequency inverter for pump rotation control. Gas flow control was performed by OMEGA mass flow meter of the FMA series. Flow visualization was done with images from a laser sheet technique in order to assess the behavior of the air bubbles as well as the water flow in the mold. SG6 particles (similar density of water) were added to visualize the water movement. The flow field was evaluated by Pivview software in order to generate the motion vectors images.

The operational range includes conditions which are similar to industrial practice (Table 1). The same holds for liquid (water) flow rate and gas specific flow rate (STP liter per minute).

A mathematical model was developed and setup using CFX in steady state (CFX 19.1, Ansys®) [13]. The refractory main features and the bubble dimensions are given in Table 2, more details of the manufacturing and experiments are described in a previous publication [7]. Following [8] the best setup for drag and non-drag forces is achieved for Grace coefficient equal to −1, coefficient of virtual mass force – CVMF – equal 0.25 and the Frave Averaged model for turbulent dispersion force – TDF –, without using wall lubrication force (WLF) and lift force. The importance of the parameters of drag and non-drag forces on gas–liquid interaction were discussed and presented by Peixoto et al. [9,15] and Liu et al. [13]. The MUSIG model [14] was adopted for breakup and coalescence of bubbles, which refines the solution and allows the mathematical simulation to represent the physical results better. Liu et al. [13] also described the MUSIG function and the equations of lift forces, VMF, TDF and WLF and used them to develop a mathematical model of bubble interaction in a slab continuous casting mold.

The mathematical model was elaborated in such a way as to represent the physical conditions of the model (Fig. 1). The water flow rate was 336 L/min and 400 L/min with the air flow rate of 12 STP L/min as determined by Santos et al. [5]. The mesh was constructed with 360,115 nodes, being more refined at the outlet of the submerged nozzle and in the jet region (Fig. 2). Inflation was used on the walls in order to obtain a better fit for the calculation of the turbulence equations in this region. Due to its symmetrical geometry and the objective of saving computational resources, only a fourth of the model was taken for simulation purposes. Simulations were done for bubble fixed diameter as well as bubble coalescence following MUSIG model.

A first set of CFD simulations was performed in order to reproduce the gas distribution in the physical model. The main objectives were to assess the suitability of combining drag and non-drag forces and MUSIG function in order to describe two phase flow in this system. A second set of simulations of the steel-argon system was then performed by CFD including the effects of drag and non-drag forces, the MUSIG model as well as the effects of gas expansion.

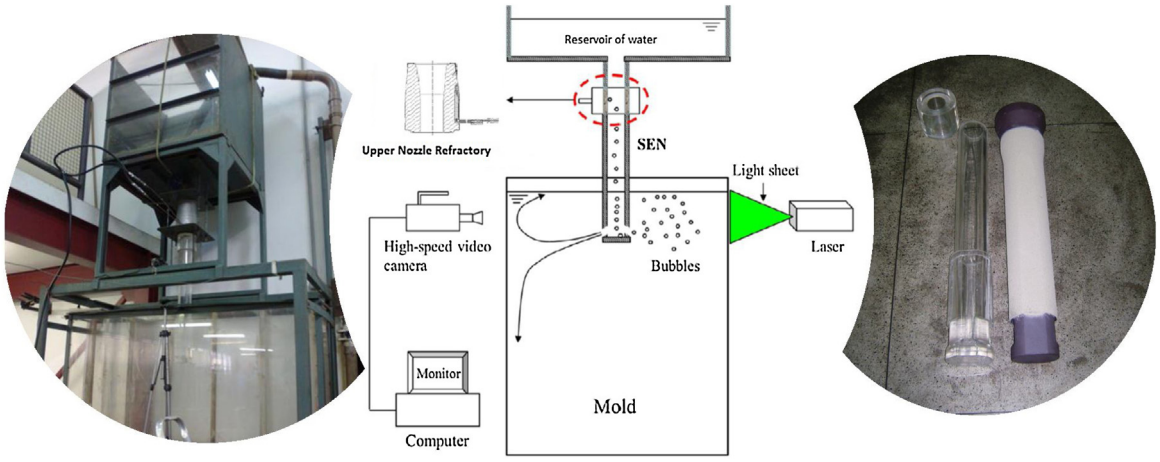

Fig. 1 – Photos of the 1:1 scale of physical model (water reservoir, upper refractory nozzle, valve for reduction and flow control SEN made of acrylic and mold) (a), assembly scheme (b) and model SEN alongside the actual SEN (c) [5].

Table 1 – Geometrical physical dimension and process conditions in the steel caster.

Dimensions	Actual caster	1:1 water model (Fig. 1)	1:1 mathematical model with two symmetry planes	
			Steel/argon	Water/air
Mold width × thickness	1260–200 mm	1260– 200 mm	630–100 mm	630–100 mm
SEN inner diameter	82 mm	82 mm	(82 mm)	(82 mm)
Length of SEN	870 mm	870 mm	870 mm	870 mm
SEN port dimensions	134–120 mm	134–120 mm	(134–120 mm)	(134–120 mm)
Nozzle bore diameter: inner/outer	79–134 mm	79–134 mm	(79–134 mm)	(79–134 mm)
Nozzle port size width/height	67- 72 mm	67- 72 mm	(67–72 mm)	(67–72 mm)
Exit angle of nozzle	15° down	15° down	15° down	15° down
Submergence depth of SEN	240 mm	240 mm	220 mm	220 mm
		Process conditions		
Liquid density	7020 kg/m^3	998.2 kg/m^3	7020 kg/m^3	998.2 kg/m^3
Liquid viscosity	0.0056 kg/m s	0.001 kg/m s	0.0056 kg/m s	0.001 kg/m s
Liquid flow rate	336–400 L/min	336–400 L/min	84–100 L/min	84–100 L/min
Gas density (at 25 °C)	1.623 kg/m^3	1.185 kg/m^3	1.623 kg/m^3	1.185 kg/m^3
Gas density (at 1600 °C)	0.47735 kg/m^3	–	0.47735 kg/m^3	–
Gas viscosity	7.42×10^{-5} kg/m s	1.85×10^{-5} kg/m s	7.42×10^{-5} kg/m s	1.85×10^{-5} kg/m s
Gas flow rate	12 STPL/min	12 STPL/min	3 STPL/min	3 STPL/min
Interfacial tension	1.5 N/m	0.0728 N/m	1.5 N/m	0.0728 N/m

Table 2 – Physical properties of porous materials used in physical model experiments and bubble size distribution for different materials [7].

Type	Bulk density (g/cm^3)	Apparent porosity (%)	Cold crushing strength (MPa)	Permeability (CentiDarcy)	Buble Size distribution water – 3 Sigma (mm)	Buble Size distribution steel (**) 3 Sigma (mm)
Refractory 1 (*)	2.54	22.14	26.28	261.5	0.6–3.2	0.9–4.8
Refractory 2 (*)	2.87	26.43	78.06	928	0.8–5.6	1.2–8.4

(*) From this point on refractories 1 and 2 will be identified as MUSIG 1 and 2, respectively.
(**) The bubble size distribution accounts for thermal expansion.

The expansion factor λ takes in consideration thermal and pressure effects and is calculated as follows [12] and [16]:

$$\lambda = \frac{Q_{1873K}}{Q_{273K}} = \left(\frac{1,013\,x\,10^5\,Pa}{1,013\,x\,10^5\,Pa + \rho_s g\,H}\right) x \left(\frac{1873\,K}{273\,K}\right) \quad (1)$$

where, ρ_s is molten steel density, and H is hydrostatic head distance from the tundish top surface to the gas channel exit.

Both set of simulations take in consideration three-dimensional and turbulent flow; incompressible Newtonian fluids, isothermal system (at 25 °C or 1600 °C), ambient pressure equal to 1 atm. Standard values for the physical properties

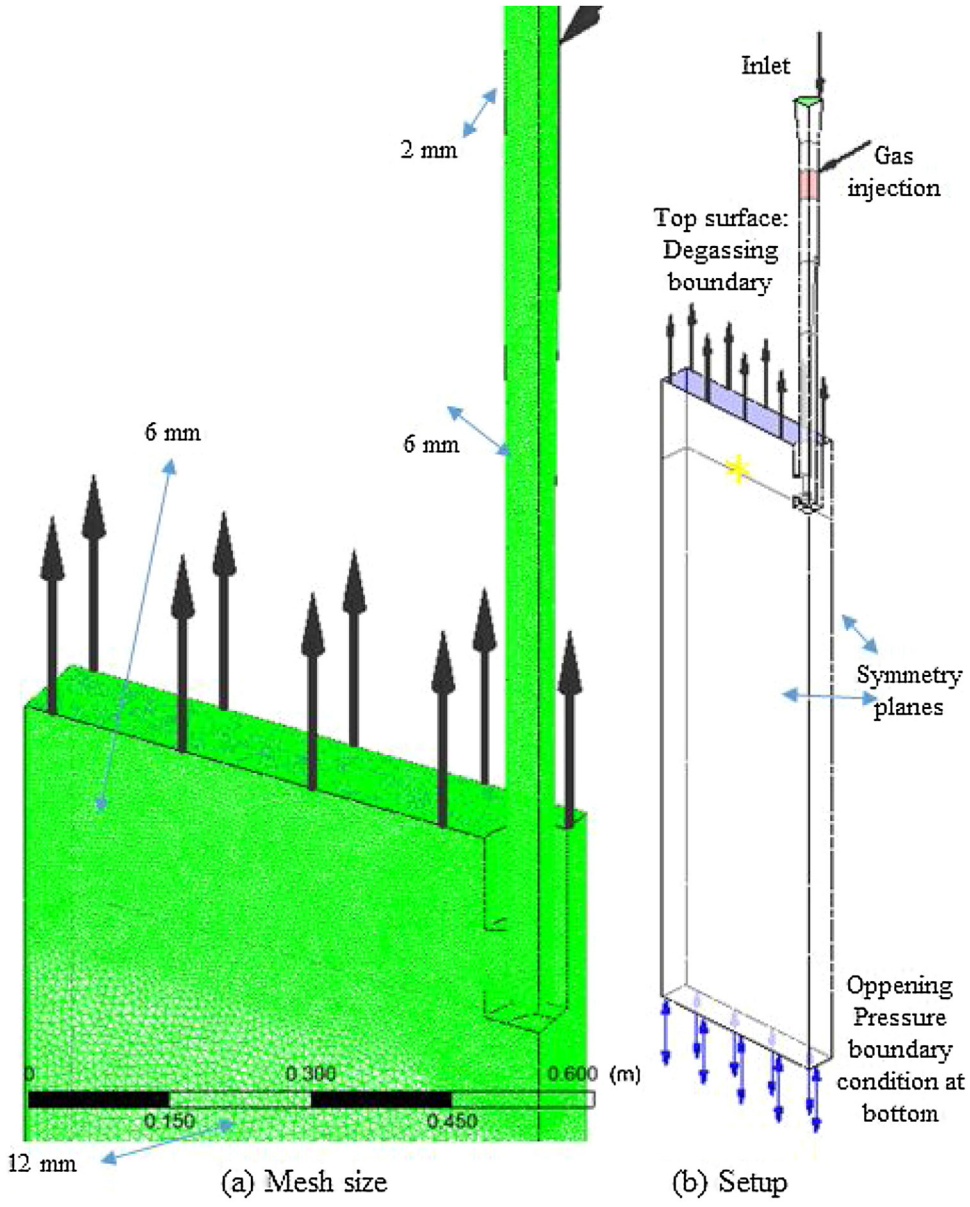

Fig. 2 – Mold and submerged nozzle: (a) mesh size; (b) setup details.

of water and air (at 25 °C) were used. Materials properties are given in Table 1. Water or molten steel is defined as continuous phase; and air or argon as the dispersed phase. Boundary conditions assume non-slip condition at every wall, which implies kinetic energy of turbulence, kinetic energy dissipation rate of turbulence and velocity are zero at these locations. At the output, region of the mixture liquid and gas, the variables are free to float being therefore determined by the mathematical code. The kinetic energy of turbulence and the rate of energy dissipation at the inlet are determined from the average velocity in the system, i.e. by the flow and cross-sectional area of flow.

3. Results and discussion

3.1. *Mathematical simulation — water/air system*

In the physical model, Fig. 3(a) and (b), 336 L/min and 12 STP L/min, it is possible to notice an upward flow near the nozzle, which disperses in opposite directions when reaching the meniscus. However, the flow towards the nozzle is of low intensity. As for the downward flow it is noted a deviation towards the narrow face of the mold. The flow displacement in the mold is a function of the dissociation of the second

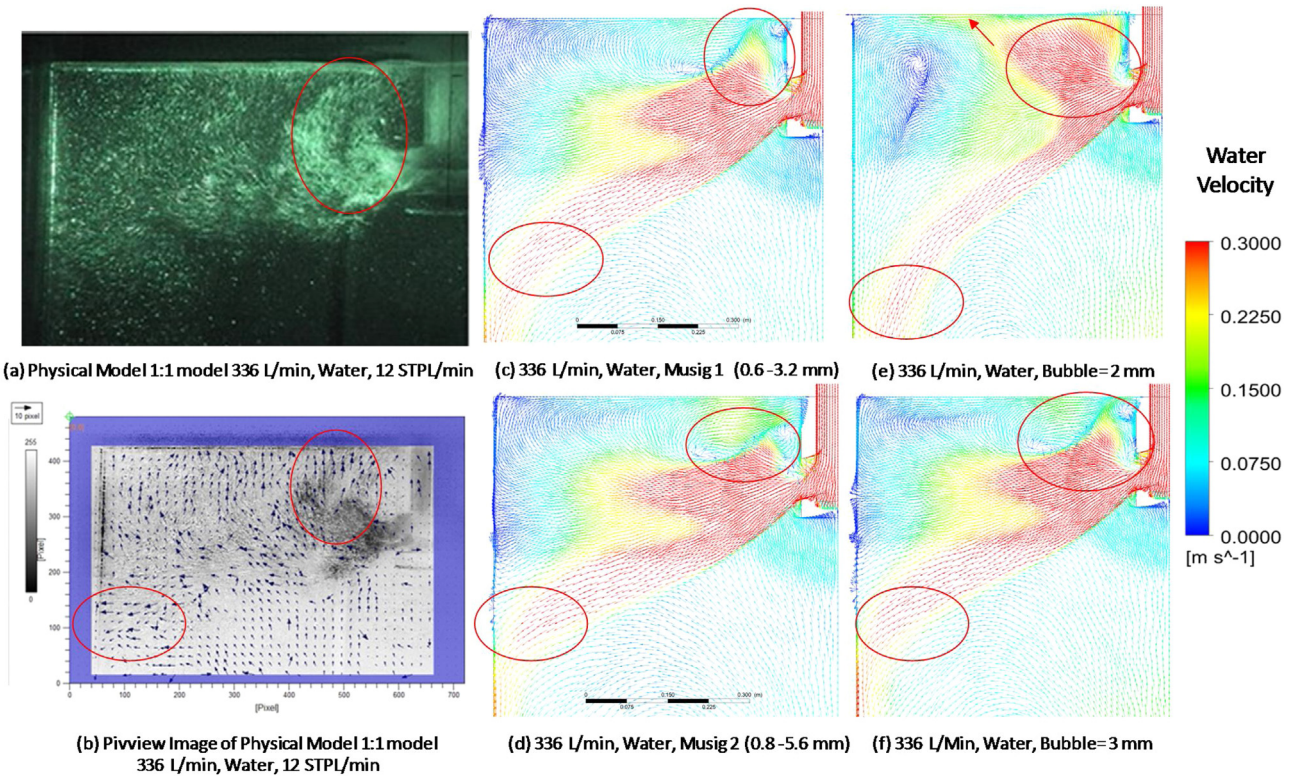

Fig. 3 – Fluid velocity, with 12 STP L/min of air for 336 L/min water: physical model half view (a) and image generated by Pivview (b) [5], MUSIG 1 = 0.6–3.2 mm (c), MUSIG 2 = 0.8–5.6 mm (d), bubble = 2 mm (e) and bubble = 3 mm (f).

phase (air) and the liquid phase (water) in the mold and the effect of buoyancy, and the drag and non-drag forces on it [5]. The MUSIG set up presented better results, Fig. 3(c) and (d), when compared to the physical model. For instance, an upward flow near the SEN with no displacement in the direction of the mold wall, and a downward flow shifted toward the mold wall. However, for the 2 mm fixed bubble condition (Fig. 3(e)), a strong upward flow near the SEN with reversal of the meniscus flow direction is observed; in addition the downward flow is not diverted towards the mold wall. For fixed bubble 3 mm (Fig. 3(f)), although it presents similar behavior to MUSIG 1 (0.6–3.2 mm) near the SEN and there is a deviation of the downward flow towards the mold, it presents superior speeds than (c) and (d) near the narrow face of mold, which may result in lower roll with higher speeds.

Changing of the water flow rate from 336 L/min to 400 L/min increases the non-continuous dispersion of phase air in the mold and enables the formation of the upper roll with a raising of meniscus velocity, as can be seen in the physical model, Figs. 4(a and b) and 5(a and b). By evaluating the ISO Volumetric surface, it is possible to identify changes regarding flow and bubble distribution.

As an example, Fig. 4(c–e) show an increase of isovolumetric surface contact at the wide face when liquid flow rate increases. It can be observed, when comparing 4(e), 400 L/min, with 4(c) and (d), 336 L/min, that there is a growth of the gas penetration into the mold. Changing the distribution of bubbles from MUSIG 1–2, with a flow rate of 336 L/min, implies in a better defined upper roll with positive impact for meniscus speed (Fig. 4(f) and (g)). This phenomenon is more significant with increasing of water flow to 400 L/min (see Fig. 4(h)), even with smaller bubble diameters (0.6–3.2 mm). The same behavior is observed when evaluating the continuous phase water via vectors generated by Pivview, Fig. 5(a) and (b), and mathematical model, Fig. 5(c–e).

Increasing the bubble size distribution (MUSIG 1–2) and the water flow (336 L/min to 400 L/min) results in an increase in the meniscus velocity towards SEN, as shown in Figs. 4(f–h) and 5(c–e), and consequent displacement of the gas plume towards the SEN (Fig. 5(f–h)). When comparing the images of the physical model Fig. 5(a, i), for 336 L/min and 12 STP L/min, with the gas concentration near the SEN, Fig. 5(f–g), it can be identified that MUSIG 1 (0.6–3.2 mm) best represents the physical model, as the bubbles have vertical rise without displacement towards the SEN.

The perspective images of the mold (Fig. 6) allow one to observe the effect of bubble diameter and water flow on the ISO Volumetric air fraction surface. Increasing the diameter of bubbles Fig. 6(a) and (b) (MUSIG 1 to MUSIG 2) leads to the displacement of the region with the highest concentration of gas on the meniscus (in green) towards the SEN; also there is an enlargement of the ISO surface contact with the wide face.

3.2. *Mathematical simulation — steel/argon system*

For the liquid steel setup condition (T = 1600 °C), 12 STP L/min argon flow, drag and non-drag forces, Grace = −1 and thermal expansion factor of 3.4, it can be noticed an upward steel flow

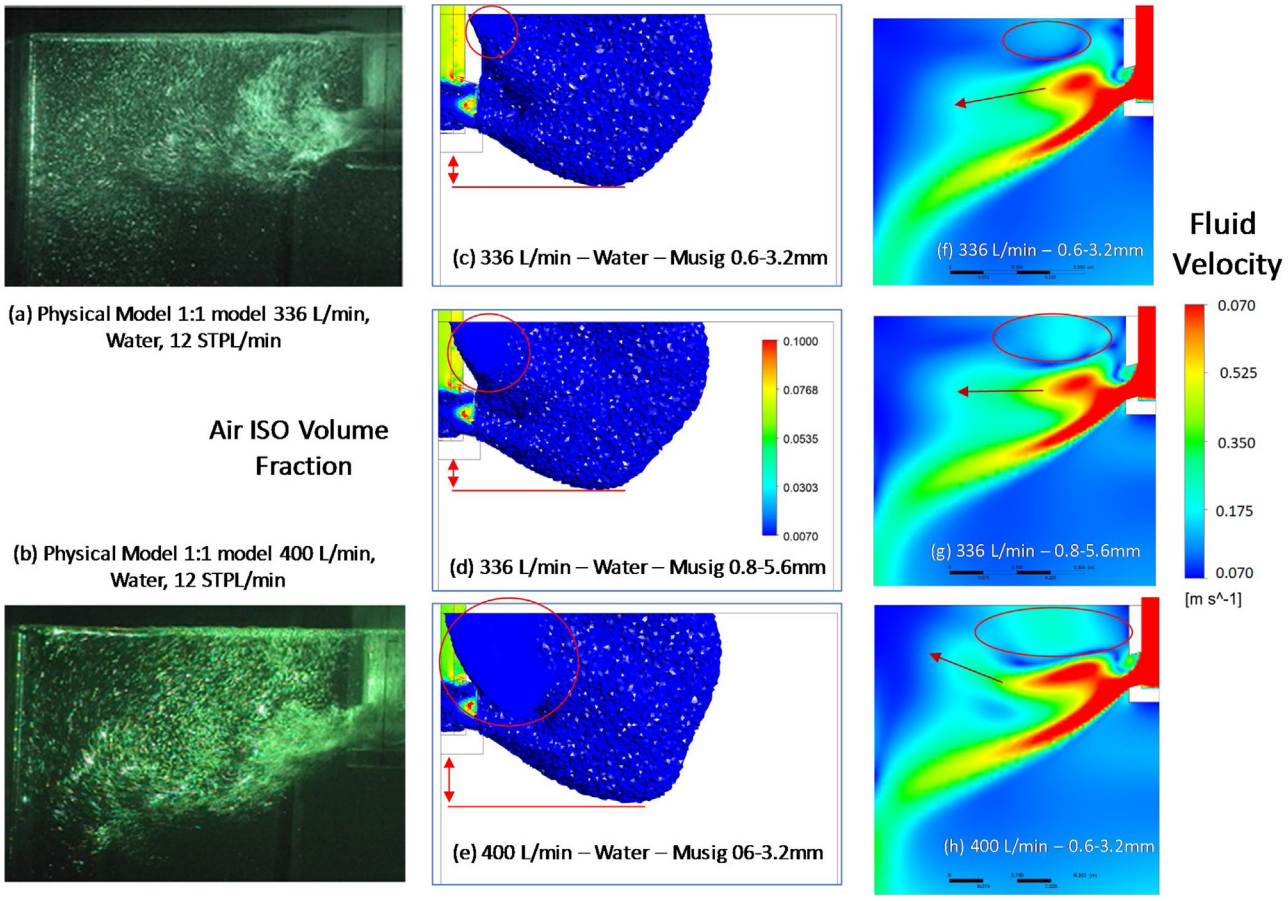

Fig. 4 – Physical and mathematical simulation with 12 STP L/min of air in a continuous phase of water, physical model with (a) 336 L/min and (b) 400 L/min [5], (c) ISO Volumetric MUSIG 1 (0.6–3.2 mm) with 336 L/min, (d) ISO Volumetric MUSIG 2 (0.8–5.6 mm) with 336 L/min, (e) ISO Volumetric MUSIG 1 — 400 L/min, and fluid velocity with (f) MUSIG 1 — 336 L/min, (g) MUSIG 2 — 336 L/min and (h) MUSIG 1 — 400 L/min.

in the mold after leaving the SEN exits that moves in the direction of the meniscus and creates a recirculation zone (inverted upper roll), between the half of the mold and the narrow face, Fig. 7(a–c). In this region it is possible to observe the formation of swirls and a probable displacement of them with risk of powder entrapment when approaching the meniscus. The Argon distribution Fig. 7(d–f) presents a behavior similar to that discussed for the water-air model with distinction for the displacement of the gas from the SEN region to the condition of 400 L/min of steel, which can be explained by reversing the direction at the meniscus.

The volumetric ISO distribution Figs. 7(g, h) and 8(a, b) (336 L/min, from MUSIG 1 to MUSIG 2) shows that an increase in bubble diameters, from MUSIG 1 to MUSIG 2, results in an slight expansion of the region with highest concentration of gas at the meniscus surface, and a smooth enlargement of the ISO volumetric surface near the SEN next to the wide mold face (see the red circles in this area). That is an increase in bubble size displaces the bubbles to the central region of the mold as it can be seen when results from MUSIG 1 and MUSIG 2 are compared.

For the condition of increasing steel flow from 336 L/min to 400 L/min, Figs. 7(g, i) and 8(a, c), both with MUSIG 1 (0.8–4.8 mm), the effects on gas distribution are more significant. As an example, there is an enlargement of the gas contact region with the mold wide face and an enlargement of the volumetric gas surface (Fig. 8(c)). There is also an increase in displacement of the gas from the SEN and a reduction in region of highest gas concentration at the meniscus surface. These observations corroborate the positive effect of increasing the steel flow on the gas distribution in the mold which in turn reduces the meniscus turbulence and consequently the opening of the powder-fluxing cover and its drag into the mold, compromising the quality of slabs. The flow rates of 336 L/min and 400 L/min were determined based on actual throughputs used in Continuous Casting of Ultra Low Carbon Steel. The flow rate of 400 L/min is the target condition for better slab quality for simulated dimensions [5]. Similar results are presented and discussed by Liu et al. [17] and [18] and have been correlated with practical observations in continuous casting of slabs.

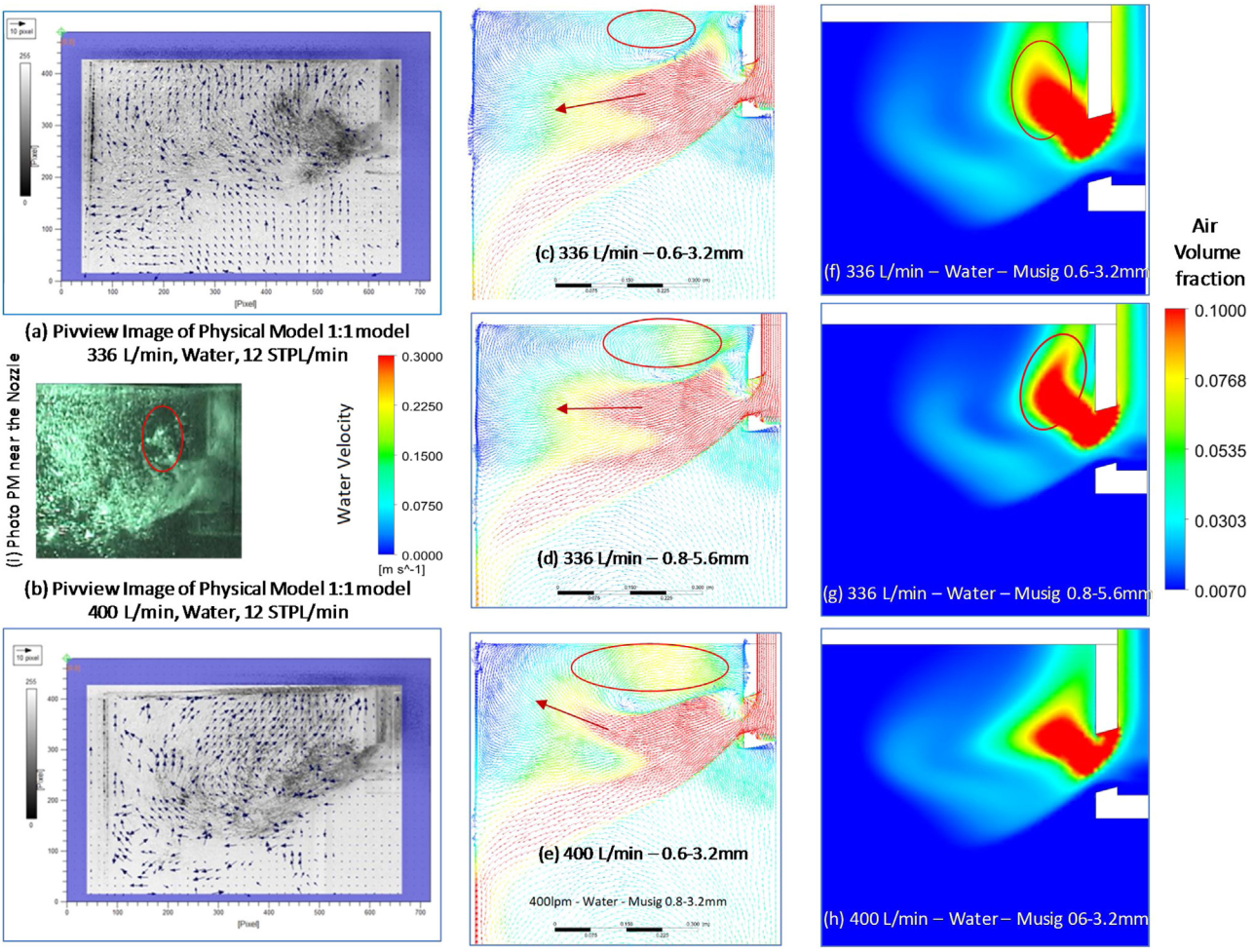

Fig. 5 – Pivview images of physical model with 12 STP L/min with (a) 336 L/min, (b) 400 L/min and mathematical simulation with water, 12 STP L/min of air, water velocity (c) 336 L/min MUSIG 1, (d) 336 L/min MUSIG 2, (e) 400 L/min MUSIG 1, and air volume fraction (f) 336 L/min MUSIG 1, (g) 336 L/min MUSIG 2, (h) 400 L/min MUSIG 1, and (i) photo of physical model near the nozzle.

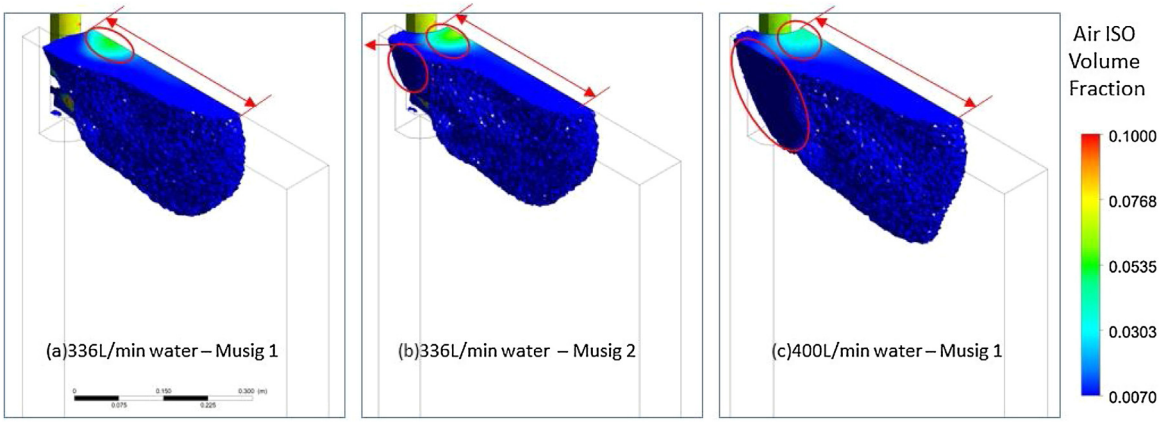

Fig. 6 – Mathematical simulation with 12 STP L/min of air. ISO volumetric surface images of (a) 336 L/min MUSIG 1, (b) 336 L/min MUSIG 2, e (c) 400 L/min MUSIG 1.

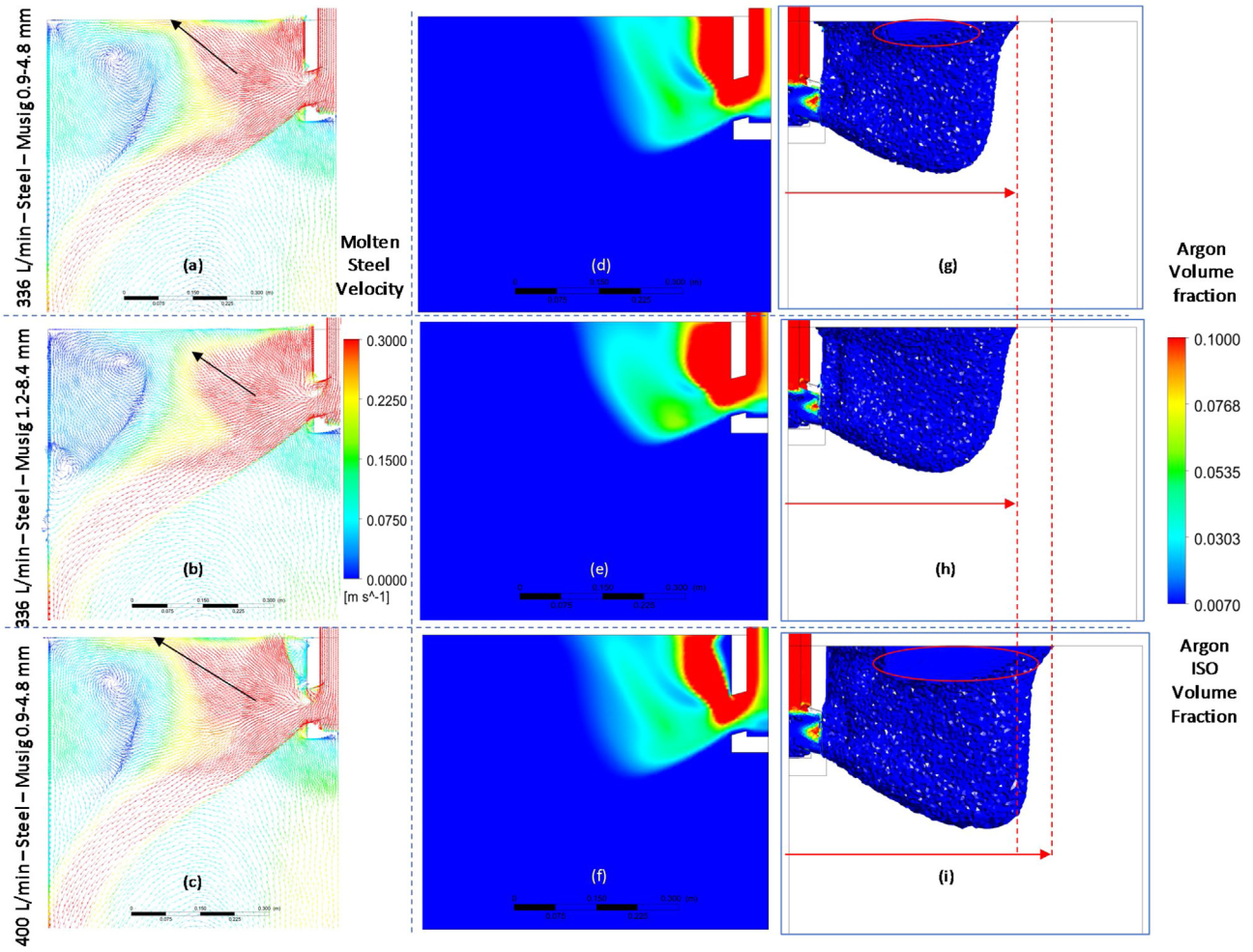

Fig. 7 – Mathematical simulation with 12 STP L/min of argon in a continuous phase of steel at 1600 °C with thermal expansion adjustment, fluid velocity (a) 336 L/min MUSIG 1 — 0.8–4.8 mm, (b) 336 L/min MUSIG 2 — 1.2–8.4 mm, e (c) 400 L/min MUSIG 1 — 0.8–4.8 mm, argon volume fraction (d) 336 L/min MUSIG 1 — 0.8–4.8 mm, (e) 336 L/min MUSIG 2 — 1.2–8.4 mm, e (f) 400 L/min MUSIG 1 — 0.8–4.8 mm, argon ISO volume (g) 336 L/min MUSIG 1 — 0.8–4.8 mm, (h) 336 L/min MUSIG 2 — 1.2–8.4 mm, e (i) 400 L/min MUSIG 1 — 0.8–4.8 mm.

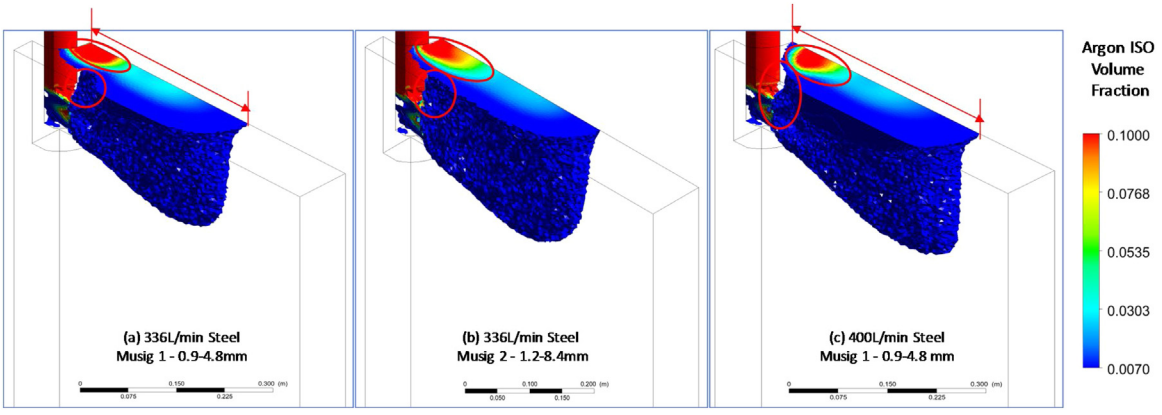

Fig. 8 – Mathematical simulation with 12 STP L/min of argon in a continuous phase of steel at 1600 °C, ISO volumetric surface images of (a) 336 L/min MUSIG 1, (b) 336 L/min MUSIG 2, e (c) 400 L/min MUSIG 1.

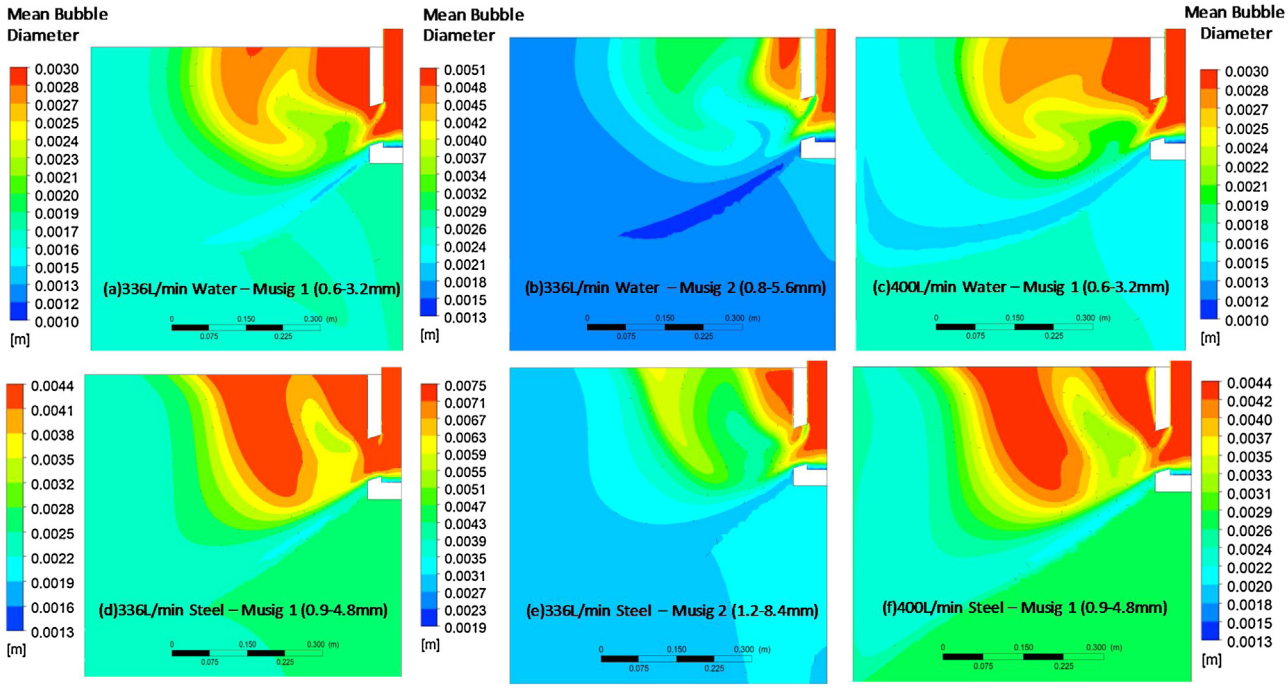

Fig. 9 – Mathematical simulation with 12 STP L/min mean bubble diameter of air in a continuous phase of water at 25 °C, (a) 336 L/min MUSIG 0.6–3.2 mm, (b) 336 L/min MUSIG 0.8–5.6 mm, e (c) 400 L/min MUSIG 0.6–3.2 mm, of argon in a continuous phase of steel at 1600 °C, (d) 336 L/min MUSIG 0.9–4.8, (e) 336 L/min MUSIG 1.2–8.4 mm, and (f) 400 L/min MUSIG 0.9–4.8 mm.

3.3. *Mathematical simulation — bubble behavior in the mold*

Fig. 9 shows the effects of the initial bubble size distribution (Table 2) and liquid flow (water or steel) on the average size of bubbles per regions in the mold. Increasing the average bubble size Fig. 9(a, b) and (d, e) implies in a reduction of the region with larger bubbles near the SEN. This can be correlated to Figs. 6 and 8 and the effect of enlargement of the gas concentration area at the meniscus surface. Also the bubble size distribution in the steel/argon and water/air models are distinct what can be explained on differences regarding bubble sizes, and phases physical properties.

Comparing Fig. 9(a) and (c), and (d) and (f), it is possible to notice that the increase of the liquid flow promotes an enlargement of the areas with larger average diameter which confirms the effect of drag of the gas by the continuous phase (steel/water) observed in Figs. 6 and 8. However, Fig. 9 also presents a possible limitation of the MUSIG function, since the size distribution remains similar in the mold even after going through the bottom of the SEN.

4. Conclusions

- It is apparent that permeability of industrial refractories and its effect on the bubble size distribution are to be taken in consideration for proper setup of mathematical models of continuous casting.
- Gas thermal expansion and a combination of drag and non-drag forces as well as models for bubble coalescence and breakage should be include in CFD simulations of continuous casting.
- MUSIG model for breakup and coalescence of bubbles refines the solution and allows the mathematical simulation to represent the physical results better when compared to fixed bubble simulation.
- The mathematical model with setup MUSIG, drag and non-drag forces, Grace = −1, presented results consistent with those observed in the physical water model.
- Refractory 1 (MUSIG 1 = 0.6–3.2 mm) was the one that best represented the condition observed in the 1:1 scale physical water model.
- The molten steel simulations predicts an upward flow at the exit of the SEN which causes the reversal of the direction of the upper roll and that would lead to the formation of swirls between the central region of the mold and the narrow face.
- The results of molten steel simulations corroborate the positive effects of increased liquid phase flow in regard to: better distribution of gas in the mold; subtle reduction in the average diameter of bubbles in the mold; reduction of swirl formation near the narrow face; and increase of velocities in the meniscus.
- The mathematical model of continuous casting with the MUSIG function showed continuous (water), dispersed (gas) and medium size bubbles compatible with those reported in the literature. However, the MUSIG function may have a restriction as the mold median bubble size distribution is similar to the setup distribution.

Conflicts of interest

The author declares no conflicts of interest.

Acknowledgements

The authors would like to thank the Research and Development Center of RHI MAGNESITA – Contagem – MG Unit, the Gorceix Foundation, CNPq, FAPEMIG, and PUC Minas (FIP Projects 1/2017-336-S1 and 1/2016-10295)

Appendix A. Supplementary data

Supplementary material related to this article can be found, in the online version, at doi:https://doi.org/10.1016/j.jmrt.2020.02.099.

REFERENCES

[1] Suzuki H, Yoshimura Y, Ogata M, Imai N. Structure of porous upper nozzle for tundish and gas bublle behavior, Shinagawa technical report, vol. 46; 2003. p. 67–76.
[2] Yuan F, Wang X, Zhang J, Zhang L. Numerical simulation of Al_2O_3 deposition at a nozzle during continuous casting. J Univ Sci Technol B 2008;15(June (3)):227.
[3] Thomas B, Dennisov A, Bai H. Behavior of argon bubbles during continuous casting of steel. In: ISS 80th Steelmaking Conference. 1997. p. 375–84.
[4] Lee G, Kim S, Thomas B. Investigation of refractory properties on the initial buble behavior in the water model of continuous casting process. In: Materials Science and Technology Conference. 2009. p. 25–9.
[5] Santos P Junior, Silva C, Silva I, Ribeiro B, Santos M. Inert gas distribution and its effect on the flux field during continuous casting of slabs: mathematical modelling. 45ª Seminário de Aciaria, vol. 45; 2013. Araxá, MG, Brasil.
[6] Liu R, Thomas BG. Model of gas flow through porous refractory applied to an upper tundish nozzle. Metall Mater Trans B 2015;46B(February):388–405, http://dx.doi.org/10.1007/s11663-014-0198-5.
[7] Santos P Junior, Silva C, Dutra P, Santos A, Carvalho B, Galinari C, et al. Influence of the refractory of the Upper nozzle in the behavior of bubbles in physical model of water — continuous casting of slabs. 49° Seminário de Aciaria, Fundição e Metalurgia de Não-Ferrosos, vol. 49; 2018. p. 363–74, http://dx.doi.org/10.5151/1982-9345-31597. São Paulo, Brasil.
[8] Santos PL Junior, Peixoto JJM, Silva CA, Silva IA, Galinari CM, Seshadri V. The effect of upper nozzle refractory in bubble behavior inside the SEN and slab mold in continuous casting: physical and mathematical model. In: The Iron and Steel Technology Conference and Exposition — AISTECH. 2019. p. 1373–82, http://dx.doi.org/10.33313/377/139.
[9] Peixoto JJM, Gabriel WV, Oliveira TAS, Barony NB, Silva CA, Silva IA, et al. Influência das Forças de Interação Líquido/Gás na Análise via CFD do Reator RH. In: 48ª Seminário de Aciaria, Fundição e Metalurgia de Não-Ferrosos. 2017. p. 356–67.
[10] Chen W, Ren Y, Zhang L, Scheller PR. Numerical simulation of steel and argon gas two-phase flow in continuous casting using LES + VOF + DPM model. JOM 2019;(71):1158–68, http://dx.doi.org/10.1007/s11837-018-3255-8.
[11] Díaz M, Iranzo A, Cuadra D, Barbero R, Montes F, Galán M. Numerical simulation of the gas–liquid flow in a laboratory scale bubble column influence of bubble size distribution and non-drag forces. Chem Eng J 2008;139:363–79.
[12] Cho S-M, Thomas BG. Effect of bubble behavior for a stopper rod with multiple side-channel injection on bubble size distributions in nozzle and mold during continuous casting of steel. In: AISTech 2019 — Proceedings of the Iron & Steel Technology Conference. 2019. p. 1317–30, 10.33313/377/135.
[13] Liu ZQ, Qi FS, Li BK, Cheungb SCP. Modeling of bubble behaviors and size distribution in a slab continuous casting mold. Int J Multiphase Flow 2016;79:190–201. China.
[14] Ansys Inc.: ANSYS CFX- Solver Theory Guide, Release 17.1, Canonsburg, PA, 2017, pp. 153-213.
[15] Peixoto JJM, Gabriel WV, Oliveira TAS, Silva CA, Silva IA, Seshadri V, et al. Numerical simulation of recirculating flow and physical model of slag–metal behavior in an RH reactor: application to desulfurization. Metall Mater Trans B 2018;49B(5):2421–34.
[16] Liu Z, Li L, Qi F, Li B, Jiang M, Tsukihashi F. Population balance modeling of polydispersed bubbly flow in continuous-casting using multiple-size-Group approach. Metall Mater Trans B 2015;46B(February):406–20, http://dx.doi.org/10.1007/s11663-014-0192-y.
[17] Liu Z, Li BK, Jiang M, Tsukihashi F. Euler-Euler-Lagrangian modeling for two-phase flow and particle transport in continuous casting mold. ISIJ Int 2014;54(6):1314–23.
[18] Liu Z, Sun Z, Li B. Modeling of quasi-four-phase flow in continuous casting mold using hybrid eulerian and lagrangian approach. Metall Mater Trans B 2017;48B(April):1248–67, http://dx.doi.org/10.1007/s11663-016-0881-9.